1. Program Director's Name, Address, Telephone Number:
Bonnie L. Firestein, Ph.D.
Department of Cell Biology and Neuroscience
Rutgers, the State University of New Jersey
604 Allison Road
Piscataway, NJ 08854
732-445-8045

2. Name of Organization/Institution
Rutgers, the State University of New Jersey
University of Pennsylvania
Princeton University/ Columbia University

3. Grant Title
Treating TBI via Astrocyte-based Approaches

4. Grant Number
09-3209-BIR-E-2

5. Grant Period Covered by the Report
June 2008-May 2012

6. Date of Submission of the Report
August 1, 2012

1. Original aims of the project.
Subproject 1: Aim 1. To examine the viability, dendritic morphology, synaptic integrity, and electrical activity of hippocampal cell cultures after injury by glutamate stimulation with or without protective uric acid or P2Y1 antagonist treatment and to assess the role of EAAT-1 in this process; **Aim 2.** To examine how protection by uric acid or P2Y1 antagonists affects neuronal morphology and synaptic protein localization *in vivo*.
Subproject 2: Aim 1. To enhance the utility and increase the throughput of a sophisticated *in vitro* TBI model appropriate for high-content screening of novel treatments by incorporation of a substrate embedded, SMEA for chronic functional (electrophysiological) analysis; **Aim 2.** To quantify the therapeutic efficacy of multiplexed treatments directed at astrocyte regulation of extrasynaptic glutamate to reduce cell death and electrophysiological dysfunction after *in vitro* TBI.
Subproject 3: Aim 1. To examine the efficacy of uric (UA) acid as a treatment for traumatic brain injury by (a) measuring changes in excitatory amino acid transporters, specifically EAAT-1, following both single and multiple dose UA treatments *in vivo*, (b) selecting the optimal doses for EAAT upregulation following UA administration and testing the efficacy of these doses for improving outcome, reducing histological damage, and altering synaptic morphology after experimental TBI, and (c) document that UA treatment leads to the subsequent reduction of slow inward currents appearing in neurons following injury, and also reduces calcium dysregulation in astrocytes after injury; **Aim 2.** To test if a P2Y1 purinergic receptor inhibitor improves outcome after TBI by (a) establishing the effective i.v. dose of MRS2179 in vivo to reduce P2Y1 activation in cortical astrocytes, (b) assessing if this dosage level leads to an improvement in neurobehavior, reduction in cell death, and restoration of synaptic morphology after experimental TBI, and (c) evaluating if P2Y1 receptor inhibition reduces the onset of calcium oscillations in astrocytes and slow inward currents in neurons after experimental TBI; **Aim 3.** To measure if a combined approach using uric acid treatment and P2Y1 receptor inhibition enhances the improvement in outcome after TBI. To accomplish this aim, we use the optimal doses developed in the previous two aims and measure the corresponding behavioral improvement, changes in neuronal cell loss, changes in synaptic morphology, and reduction in the appearance of slow inward currents in neurons after the combined therapeutic approach.
2. Project successes. We have had enormous success with this project and share some of our many results below. We limit this summary to our most recent results as we have submitted extensive detailed progress reports in the past years:
Subproject 1: Rutgers University: We previously showed data that suggest that neurons with weakest and strongest connectivity are at highest risk of glutamate-induced toxicity while those with moderate connectivity are least susceptible. These data were published in Kutzing et al., 2011. As discussed in our last progress report, we were continuing to screen compounds that would protect neurons from glutamate-induced toxicity. Our results on memantine are shown below and have been published in Kutzing et al., 2012. We analyzed the effect of glutamate treatment with or without memantine treatment on the pattern of action potential firing of the neuronal network. We performed this assessment 24 hours after treatment as this is the time point we previously used to assess the effects of glutamate treatment both cellularly[14] and electrophysiologically[22]. The synchronization index (SI) was calculated between all pairs of electrodes before and after glutamate and memantine treatments in order to measure changes in the synchronization of neuronal firing throughout the neuronal network. This resulted in a matrix in which each electrode is plotted against all other electrodes, yielding a 59 x 59 matrix (Figure 1). In control cultures and in cultures treated with glutamate and memantine simultaneously, a large percentage of the electrode pairs showed either no change in the SI or an increase in the SI (Figure 1, 1st and 3rd rows). In cultures treated with 300 µM glutamate, the majority of electrode pairs showed a large decrease in the SI (Figure 1, 2nd row). Treatment of cultures with 50 µM memantine prior to glutamate treatment also resulted in decreases in the SI of many electrode pairs (Figure 1, 4th row). However, these decreases were not as great as cultures treated with glutamate alone. In addition, in these cultures, there were a number of electrode pairs that did not show a change in the SI before and after drug treatments. The 58 SI values for each electrode were averaged in order to calculate an average synchronization index (ASI) for each electrode. The SI value of the electrode with itself and with the reference electrode was excluded. This resulted in a matrix where the locations of the ASI values represent the actual physical location of each electrode (Figure 2). The change in ASI grids for each of the experimental groups is similar to those seen in the SI grids (Figure 1) except that increases and decreases in ASI values are reduced, because in this analysis, the individual SI values were averaged. In control cultures and in cultures simultaneously treated with glutamate and memantine, the ASI values of the electrodes either did not change or increased slightly. For cultures treated with 300 µM glutamate or pretreated with 50 µM memantine and then treated with 300 µM glutamate, the ASI value of a large number of electrodes decreased, with larger decreases occurring for the culture treated with only 300 µM glutamate. The SI values of all of the MEAs before and after drug treatments of each experimental group were combined in order to quantitatively measure changes in the synchronization of action potentials resulting from treatment with glutamate (Figure 3). The values were normalized to the SI before drug treatment. There was a significant decrease in synchronization in cultures treated with 300 µM glutamate. Cultures treated with memantine, either prior to glutamate treatment or at the same time as glutamate treatment, completely protected this overall loss in synchronization. There was a trend towards a decrease in synchronization in cultures treated with memantine prior to glutamate treatment, but the decrease was not significant. To determine if the initial level of synchronization of action potential firing between two electrodes determines the ability of memantine to protect their synchronization, the CS values between all electrode pairs of each treatment group were normalized to the initial SI value and binned into 3 groups depending on the initial SI value: 0.1-0.4 (weak initial synchronization), 0.4-0.7 (moderate initial synchronization) and 0.7-1 (strong initial synchronization) (Figure 4). Cultures treated with 300 µM glutamate resulted in a loss of synchronization of action potential firing in all groups. Treatment with memantine at the same time as glutamate treatment completely protected all losses in synchronization resulting from

glutamate treatment. Treating cultures with 50 µM memantine before glutamate treatment completely protected the loss of synchronization of firing of electrode pairs that were initially weakly and moderately synchronized. Pretreatment with memantine was able to partially protect the synchronization of activity of electrode pairs that were initially strongly synchronized, as the loss in synchronization was significantly greater than the control but significantly less than cultures treated with only glutamate. We assessed whether treatment with glutamate affects the shape of the SBEs, specifically whether it affects the length or duration of the bursts, and whether memantine treatment can prevent these effects. The average burst duration of all the bursts on a single MEA was calculated and combined with the averages of all of the other MEAs treated with that glutamate concentration (Figure 5). We found a significant increase in the burst duration of cultures treated with 300 µM glutamate as compared to control cultures. When memantine was applied at the same time as glutamate, the increase in burst duration was completely blocked. However, pretreatment of cultures with memantine did not prevent the increase in burst duration resulting from glutamate treatment. Rastor plots of example SBEs for each of the treatment groups are shown in Figure 6. In order to further investigate the mechanism by which the burst duration is increased in injured cultures, we recorded the activity of both untreated control cultures and cultures treated with 300 µM glutamate while in a solution of 10 µM bicuculline diluted in recording media. After allowing the cultures to equilibrate in this media for ten minutes, we recorded the culture activity and compared the duration of bursts of each MEA in regular recording media and in the presence of bicuculline. The application of bicuculline to cultures injured with 300 µM glutamate did not change the width of the bursts. In control cultures, bicuculline consistently resulted in a dramatic increase in burst duration, similar to what is seen after GIE. Our collaborative work with David Meaney that achieves our initial aims is presented in the University of Pennsylvania section.

Subproject 2: Columbia University/Princeton University: Columbia University: Uric Acid Neuroprotection after Mechanical Injury: Treatment with 300 µM uric acid immediately after mechanical injury or with 30uM immediately after or 30 min after mechanical injury significantly reduced cell loss in hippocampal brain slice cultures (Figure 1, Table 1). In our *in vitro* model of traumatic brain injury (TBI) in which organotypic brain slice cultures are injured by a precisely controlled deformation, cell death is delayed and progressive. Cell death typically begins after 1d post-injury and then progresses to a plateau at 4d post-injury. Vehicle treated, injured cultures displayed this typical progression of cell death. In contrast, treatment with 300 µM or 30uM uric acid halted the progression of cell death between 3 and 4 days after injury. The effect was widespread throughout the hippocampus with protection demonstrated in CA1, CA3, and dentate gyrus (DG) regions. These results are exciting because they are the first to demonstrate that uric acid may be neuroprotective after TBI. MRS2179 Neuroprotection after Mechanical Injury: Treatment with 30 µM MRS2179 immediately after mechanically injury prevented the progression of cell death. Cell death was reduced at 3 and 4 days post-injury. Uric Acid Preserves Neuronal Function after Mechanical Injury: Treatment with 300 µM uric acid 60 min or treatment with 30uM uric acid immediately or 30 min after mechanical injury of organotypic hippocampal slice cultures preserved neuronal function measured at 4d post-injury. This was true for evoked activity in response to stimulation of the CA3 region (Figure 2, Table 2) or after stimulation in the DG(Figure 3, Table 3). The maximal responses (R_{max}) elicited from injured treated cultures were greater than those of injured, vehicle treated cultures, indicating that more neurons were function with treatment. In addition, the stimulus required to evoke a half maximal response (I_{50}) was lower in injured, treated cultures compared to injured, untreated cultures. This parameter, I_{50}, is independent of the number of neurons firing and provides insight into the functionality of the cellular machinery responsible for neurotransmission. These data suggest that uric acid treatment preserved the neuronal network in a more functional state compared to the untreated cultures. Taken together these results are extremely exciting and suggest that uric acid is not only neuroprotective (i.e. prevents cells from dying), but that the neurons which are preserved are functional and capable of firing action potentials. Stretchable Microelectrode Arrays (SMEA): Using the SMEAs developed by Princeton, we were able to record neural activity after mechanical stretch injury and modulate that response pharmacologically. After an 18% strain stretch injury, I_{50} – a measure of neuronal excitability – increased in the CA1, CA3, and DG hippocampal regions (Figure 4), while R_{max} – a measure of how many neurons are firing in a coordinate fashion – decreased in all regions (Figure 5), results that are consistent with our findings using conventional, rigid, glass MEAs. Additionally, we were able to combine pharmacology with mechanical deformation to modulate the neural activity of the tissue slice. Population spike frequency (Figure 6) and amplitude (Figure 7) both increased after an 18% strain injury, but was almost entirely abolished by the introduction of CNQX, an AMPA/kainate receptor antagonist. Within the same tissue slice, introducing bicuculline, a $GABA_A$ receptor antagonist, brought back the population spikes and, in fact, amplified the response compared to pre-injury, baseline levels. Performing these robust experimental techniques in one single *in vitro* platform will enable us to investigate TBI mechanisms and pathologies that we've not been able to before. **Princeton University:** Figures 1 and 2 are photographs of the most advanced stretchable microelectrode array. The array has 28 active electrodes and two reference electrode. Figure 1 demonstrates the stretchability of the array. Figure 2 shows an array to which a plastic cylinder has been attached to from a growth well. These array were used in the laboratory of Prof. Morrison for culturing brain slices and monitoring their neural activity before, during, and after stretching, and after pharmacological intervention. The project was successful.

Subproject 3: University of Pennsylvania: *In vivo* imaging of astrocyte response to mechanical trauma: Our imaging data from the first year showed that astrocytes respond to a localized mechanical impact to the cortex by showing an increase in cytosolic calcium. We provide a summary of the microcortical impact technique in Figure 1. In the past year, we verified the role of purinergic receptors in mediating this response by blocking all purinergic receptors with apyrase, a compound accelerating the breakdown of ATP. Apyrase treatment significantly attenuated the impact-mediated calcium increase (Figure 2). An alternative pathway for the calcium transients – through intercellular gap junctions – did not

significantly contribute to the measured impact response (see no response to flufenamic acid treatment; Figure 2C). These data suggest that astrocytes have a primary response in the mechanically injured brain that may persist and contribute to the long term neurocognitive deficits that appear after TBI. Astrocyte calcium waves in the penumbra can influence the activity of injured neuronal networks. We next tested if intercellular calcium waves within astrocytes of the mechanical penumbra influence the activity of neuronal networks. We first confirmed that an electrical activity pattern could be deduced from calcium imaging by measuring the simultaneous calcium imaging/MEA activity patterns in neuronal-glial cultures grown on microelectrode arrays (Fig. 4). Subfields near an electrode from a neuron identified from calcium imaging (Fig 4A; array n. 45) illustrates fluo-4 fluorescence before and during (C) a calcium transient. To draw equivalent comparisons in time between the MEA and calcium imaging, we binned the electrical activity into the same framing acquisition rate for the calcium imaging (4E, F), developed a correlation analysis between peaks in the calcium imaging and the binned MEA activity pattern (4I), and developed a critical distance correlation to achieve consistency between the MEA and the calcium imaging data (4J). On average, approximately 90% of the MEA spikes can be correlated with neuronal activity within a radial distance of 200µm from the electrode. After establishing this fidelity between the calcium imaging and electrode array measures, we used the calcium imaging to detect changes in activity after mechanical injury. In uninjured mixed neuronal-glial cultures, functional multi-neuronal calcium imaging revealed spontaneous activity among neuron clusters (Fig. 5A-E), Following mechanical injury, astrocyte intercellular calcium waves appeared in the mechanical penumbra (Fig. 4F) and both the spontaneous synchronous frequency and degree of synchronization decreased significantly in the mechanical penumbra with the onset of the intercellular wave ($P<0.01$, Fig 5G vs. 5H; 5L, 5M). Similar to pure astrocyte cultures, pretreating mixed cultures with either BAPTA-AM, PPADS, or apyrase blocked the calcium wave from appearing in astrocytes within the mechanical penumbra (Fig. 5I) and maintained post-traumatic neuronal activity at a level similar to pre-injury values (Fig. 5J vs. 5K; Fig 5L-M; for both metrics: $P>0.2$ when treated with BAPTA-AM; $P>0.1$ when treated with PPADS+Apyrase). <u>Consequences and treatment of traumatic brain injury in mice</u>: Based on the response of the living cortex to traumatic mechanical injury, we next developed methods to assay the potential improvement in outcome following treatments directed to a specific class of purinergic receptors, the P2Y1 population. We used a specific antagonist to the population (MRS2179) that showed efficacy in a slice culture model of traumatic brain injury (see Princeton/Columbia summary). Our first objective was to develop an accelerated version of the Morris Water Maze test to detect early improvement in outcome following treatment after traumatic brain injury. The Morris water maze (MWM) is an established method that is used to detect cognitive impairment in mice following experimental brain injury. The standard MWM technique for assessing learning acquisition after brain injury in mice requires testing over a protracted 4 day time course, with the trials often extending to 14 days post-injury. We developed an abbreviated MWM learning protocol administered within a single day that can be applied to evaluate the early changes (72hr post-injury) following experimental brain injury, with the long term goal of using the accelerated protocol to screen therapeutics for treating traumatic brain injury. Mice were subjected to a traumatic brain injury using controlled cortical impact (CCI). Animals were then tested in the Morris Water Maze at either 3 or 7 days post-injury. The test protocol had each mouse find a hidden platform over eight (8) consecutive trials with the start direction alternating (north, south, east and west) for each trial. The time to find the platform was recorded for each trial. The last four trials were averaged together to create a latency score for a given animal. Mice who failed to find the platform for all four trials were excluded. Analysis of variance followed by Tukey posthoc testing was used to detect differences between groups. Injury categories included sham (craniotomy only, no injury), mild (craniotomy and injury at 1 mm depth and 2.1-2.6 m/s), and moderate (craniotomy and injury at 1 mm depth and 5.5-6.4 m/s). We found that CCI produces a significant increase in accelerated MWM latency at 3d and 7d, following injury. Average latency to reach platform (seconds) for sham (n=8), mild (n=6) and moderate (n=6) injury mice at 3 days and 7 days (mild n=7, moderate n=8) post-injury, were significantly different from sham, and indicated that the accelerated MWM protocol would provide the resolution needed to detect early changes in impairment after TBI (Figure 6). We next tested if these deficits corresponded to an alteration in degenerating neurons within the hippocampus. Many techniques are available to evaluate neuronal loss, and we chose a common fluorescent label (Fluorojade; FJ) that highlights degenerating neurons throughout the brain. A common area of FJ+ neurons appears the Figure 7. We found the progressive increase in FluorJade labeling within the medial cortex 3d following injury, but this labeling decreased at 7d following injury. Although we could detect a difference in FJ+ labeling between the injured and uninjured animals, we did not detect a significant difference in FJ labeling 7d after injury. Therefore, we pursued an alternative strategy that would provide us a more distinct labeling of neurons after TBI – using a fluorescent Nissl stain. Using a fluorescently conjugated Nissl stain and GFAP immunohistochemistry, it was clear that progressive thinning occurs in the pyramidal cell layer (CA3) of the ipsilateral hippocampus 7d after injury, accompanied by changes in astrocyte reactivity with the injured and contralateral hemisphere. This thinning of the ipsilateral hippocampus coincides with cortical neuronal loss in the same hemisphere at earlier times (3d) after injury. Measures of the glial reactivity in the same animal showed that GFAP immunoreactivity was largely absent from the contralateral cortex, but was detected bilaterally in the hippocampus 7d after injury. Not surprisingly, the ipsilateral hippocampus also showed signs of reactive astrocytes. <u>*In vivo* neuroprotection studies:</u> With these accelerated methods of detecting neurobehavioral changes after TBI, we next completed our testing of a specific antagonist compound (MRS2179) at both early (3d) and more delayed (7d) times following injury. In our progress report last year, we showed the potential (n=4 animals) to improve outcome after an osmotic pump infusion of 1mM MRS2179 in the traumatically injured brain. We now show that MRS2179 treatment significantly improved outcome at 3d and 7d survival timepoints, using the accelerated Morris Water Maze paradigm described above (Figure 8). The MRS2179 compound is a very targeted compound towards

the purinergic receptors, and suggests that gliocentric mechanisms may contribute to the postinjury sequelae after TBI. Given the proof of principle with the MRS2179 treatment, we next expanded our in vivo work to study the effect of inosine treatment after TBI. We first conducted a series of pilot studies, where inosine or inosine + potassium oxanate was injected twice daily into mice. Three days following the twice daily injection protocol, we evaluated different brain regions for the presence of EAAT-2, a glutamate uptake transporter that is upregulated in spinal cord after inosine treatment. We found that both inosine based treatments increased significantly the level of EAAT-2 in the cortex and hippocampus, with the potassium oxanate + inosine showing the greatest enhancement. Given these data on the importance of combining potassium oxanate with inosine to achieve an upregulation of EAAT-2 in the brain, we next tested if this treatment would affect the normal performance of animals in the Morris Water Maze platform test. Initial studies using separate injections of potassium oxanate and inosine showed a dramatic increase, or worsening of performance, with this combined treatment. However, additional control animals injected twice with saline showed the same performance deficit, suggesting that it was the injection protocol and not the drug treatment that caused the effect originally observed in the MWM testing. To this end, we re-tested animals with a single injection of either inosine alone or a combination of inosine and potassium oxanate and found no significant difference in MWM performance with either saline injection animals or naïve animals. We used this single dose paradigm and extended it into a single injection of potassium oxanate+inosine, delivered 2x daily, over the course of several days. We observed a progressive decline in MWM testing performance when the animals received this continuous injection paradigm, with the deficits increasing over time of injection (3d, 7d, 10d; Figure 9). We chose the single dose of inosine+potassium oxanate from the above optimization studies and conducted a treatment trial in brain injured mice. For comparison, we also administered potassium oxanate and inosine as separate treatments in additional treatment groups. For all treatment paradigms, we used a single injection of drug 30 minutes after cortical impact injury, evaluating MWM performance deficit at 4d (Figure 10) and 7d (Figure 11) after injury. We did not see a significant improvement in any of the MWM deficits after treatment.

3. Project challenges. Although we have been very productive, no project is without challenges. We found that uric acid is protective in slices but has inconsistent effects in dissociated culture. In addition, delivery of uric acid by tail vein injection can be harmful to the animal, and we could not get the animals to take it orally. MRS2179 appears to be a more promising treatment as evidenced by our data. Lastly, we are still optimizing adherence of dissociated cultures to stretchable MEAs. The principal challenges encountered were (i) initial low fabrication yield of functional microelectrode arrays, (ii) initial difficulty in identifying a sterilization procedure for the arrays that did not damage them, and (iii) the need for substantially larger numbers of arrays than can be fabricated in an academic setting. Challenges (i) and (ii) were successfully overcome. The response to challenge (iii) is a plan for starting a company that will mass produce stretchable microelectrode arrays.

4. Implications for future research and/or clinical treatment. This work provides a new therapeutic target for treating TBI. To our knowledge, no group has targeted the P2Y1 receptor as a potential target, and our data is the first to shows its efficacy. We are very interested in pursuing if this is therapy works across the TBI severity spectrum, and if this therapy works when delivery is delayed. In addition, our new data suggest that memantine, and FDA approved drug, may have utility in treating patients who have experienced TBI. During the course of this project the feasibility and functionality of stretchable microelectrode arrays were demonstrated. The arrays are a new tool for the study of traumatic injury. The most appropriate future research from the fabrication point of view is to work out a reproducible manufacturing procedure that results in high product yield. This will be done best in a corporate setting.

5. Plans to continue the research, including applications submitted to other sources for ongoing support. Explain how you have leveraged NJCBIR funding to obtain additional federal or other support for brain injury research and list the appropriate funding organizations. Bonnie Firestein and David Meaney have applied for funding from the American Heart Association for screening of compounds to relieve synaptic and neurobehavioral deficits in a mouse model of TBI. Bonnie has also presented the work resulting from this grant funding to Mona Hicks, Program Director at NINDS, to discuss future opportunities for funding from NIH. Other grants submitted or funded include “Gliocentric approaches for treating traumatic brain injury,” NIH RO1, D. Meaney, PI (pending), “Blast induced thresholds for neural networks” (funded; Depart of Defense, Army Research office), “Optimizing small molecule designs to manipulate cypin levels in the injured brain to improve recovery after stroke and TBI, Planned for R21 submission in Fall 2012. Dr. Oliver Graudejus, a former senior researcher on the Princeton project, is exploring avenues to raising funding for a startup company, which will scale up the fabrication of microelectrode arrays. Dr. Graudejus is seeking funding from Federal Government SBIR sources.

6. List and include a copy of all publications emerging from this research, including those used in preparation.

Conference Proceedings:

1 Goletiani C, Morrison III B (2010) Uric acid prevents traumatic cell death and neuronal dysfunction in organotypic hippocampal slice cultures. In: Northeastern Bioengineering Conference.

2 S.P. Lacour, I. Graz, D. Cotton, S. Bauer, S. Wagner, "Elastic Components for Prosthetic Skin," Conf. Proc. IEEE Eng. Med. Biol. Soc., 8373-8376 (2011).

Abstracts:

1. Kang, W.H., Yu, Z., and Morrison III, B., Changes in electrophysiological function after controlled deformation of hippocampal slice cultures, in BMES. 2011.

2. Kang, W.H., Yu, Z., and Morrison III, B., Changes in electrophysiological function after controlled deformation of hippocampal slice cultures, in J.Neurotrauma. 2011.

3. Kang, W.H., Yu, Z., and Morrison III, B., Quantification and prediction of electrophysiological function in the hippocampus after in vitro traumatic brain injury, in J.Neurotrauma. 2012.
4. Goletiani, C., Yu, Z., Graudejus, O., Cao, W., Wagner, S., and Morrison III, B., The stretchable microelectrode array: Recent progress on a compliant interface for brain tissue, in Material Research Society. 2010.
5. Kutzing MK, Meaney DF, Morrison B 3rd, Wagner S, and Firestein BL. (2009) The Functional Recovery of Neurons after Traumatic Brain Injury. SFN Annual Meeting, 2009, Chicago, IL.
6. Kutzing MK, Langhammer CL, and Firestein BL (2010) The Functional Recovery of Neurons after Traumatic Brain Injury. BMES.
7. Kutzing MK and Firestein BL (2010) Functional assessment of neurons: applicability to stem cell-derived neurons and glia. Northeast Regional Meeting (NERM 2010) of the American Chemical Society.

Conference talks, and seminars.

1. J. Jones, Elastically Stretchable Two-level Metallization, Electronic Materials Conference 2009.
2. S. Wagner, Flexible and stretchable electronic surfaces: Materials and designs, ICAM 2009.
3. W. Cao, Mechanical and Thermal Stretching of Elastomeric Conductors, EMC 2009.
4. W. Cao, Highly stretchable encapsulated elastomeric conductors, MRS Spring 2009.
5. P. Goerrn, A taxonomy of wrinkling and cracking of hardened PDMS surfaces, MRS Spring 2010.
6. P. Goerrn, Self-organized Structures on PDMS for Large Area Optical Applications, MRS Spring 2010.
7. S. Wagner, Making gold elastic and silicon dioxide flexible, Stress Workshop 2010.
8. W. Cao, Electrical resistance of stretchable electrodes: - surface morphology - computer modeling, EMC 2010.
9. W. Cao, Electrical, mechanical, and thermal studies on stretchable electrodes, MRS Fall 2010.
10. S. Wagner, Elastically stretchable metallization for interconnects, MRS Fall 2011.
11. W. Cao, Modeling the electromechanical properties of stretchable electrodes for bioapplications,MRS Spring 2011.
12. W. Cao, Stretchable Thin Film Electrode Arrays for Neuroscience Research, U. Texas-Dallas 2011.

Conference posters.

1. J. Jones, Two-tiered stretchable conductors on elastomeric substrates, FlexTech 2009.
2. O. Graudejus, The Critical Strain of Elastically Stretchable Thin Film Metal Interconnects, FlexTech 2009.
3. W. Cao, Processing of Vias in Elastically Stretchable Microelectrode Arrays, FlexTech 2009.
4. W. Cao, Electrical, mechanical and thermal studies on stretchable electrodes - potential application for e-skin, FlexTech 2010.

Theses.

1. Irene H. Hu, Strechable Microelectrode Arrays for Spinal Cord Injury Studies, Senior Thesis, Princeton 2008.
2. Joyelle Elizabeth Jones Harris, Elastically Stretchable Thin Film Conductors on an Elastomeric Substrate, Ph.D. thesis, Princeton 2010.
3. Melinda Kutzing, DEVELOPMENT OF AN *IN VITRO* TOOL TO MEASURE THE FUNCTION OF NEURONS PROTECTED FROM GLUTAMATE-INDUCED EXCITOTOXICITY, Ph.D. thesis, Rutgers University, 2011.
3. Wenzhe Cao, Fabrication and Modeling of Stretchable Electrodes for Traumatic Brain Injury Research, Ph.D. thesis draft, Princeton, July 2012.

Publications:

1. "Characterization of an Elastically Stretchable Microelectrode Array and Its Application to Neural Field Potential Recordings," O. Graudejus, Z. Yu, J. Jones, B. Morrison III, and S. Wagner, *J. Electrochem. Soc.,* 156, P85-P94 (2009).
2. "Neural sensing of electrical activity with stretchable microelectrode arrays," Zhe Yu, Oliver Graudejus, Stéphanie P. Lacour, Sigurd Wagner, Barclay Morrison III,*IEEE Proc. EMBC,* 2009.
3. Oliver Graudejus, Patrick Görrn, and Sigurd Wagner, "Controlling the Morphology of Gold Films on Poly(dimethylsiloxane)," Applied Materials and Interfaces, 2, no. 7, 1927–1933 (2010).
4. Patrick Görrn and Sigurd Wagner, "Topographies of plasma-hardened surfaces of poly (dimethylsiloxane)," J. Appl. Phys. 108, 093522 (2010).
5. 5. Kutzing, M.K., Luo, V. and Firestein, B.L. (2011) Measurement of Synchronous Activity by Microelectrode Arrays Uncovers Differential Effects of Sublethal and Lethal Glutamate Concentrations on Cortical Neurons. Annals of Biomedical Engineering, 39(8):2252-62.
6. 6. Panzer MB, Matthews KA, Yu AW, Morrison B 3rd, Meaney DF, Bass CR. (2012) A Multiscale Approach to Blast Neurotrauma Modeling: Part I - Development of Novel Test Devices for in vivo and in vitro Blast Injury Models.
7. Front Neurol. 3:46.
8. Morrison B 3rd, Elkin BS, Dollé JP, Yarmush ML. (2011) In vitro models of traumatic brain injury. Annu Rev Biomed Eng. 13:91-126.
9. J. Harris, O. Graudejus, S. Wagner, "Elastically Stretchable Insulation and Bilevel Metallization and Its Application in a Stretchable RLC Circuit," Journal of Electronic Materials: 40, 1335-1344 (2011).
10. P. Görrn, W. Cao, S. Wagner, "Isotropically stretchable gold conductors on elastomeric substrates," Soft Matter 7, 7177-7180 (2011) DOI: 10.1039/C1SM05705G
11. Patrick Görrn, Marcus Lehnhardt, Wolfgang Kowalsky, Thomas Riedl, and Sigurd Wagner, "Elastically Tunable Self-Organized Organic Lasers," Advanced Materials 23, 869–872 (2011).

12. W. Cao, P. Görrn, and S. Wagner. “Modeling the electrical resistance of gold film conductors on uniaxially stretched elastomeric substrates, Appl. Phys. Lett. 98, 212112 (2011); doi:10.1063/1.3594240.
13. Effgen GB, Hue CD, Vogel E 3rd, Panzer MB, Meaney DF, Bass CR, Morrison B 3rd. (2012) A Multiscale Approach to Blast Neurotrauma Modeling: Part II: Methodology for Inducing Blast Injury to in vitro Models. Front Neurol. 3:23.
14. 9. Kutzing, M.K., Luo, V. and Firestein, B.L. (2012) Protection from glutamate-induced excitotoxicity by memantine. Annals of Biomedical Engineering 40(5):1170-81.
15. 10. Graudejus, O., Morrison III, B., Goletiani, C., Yu, Z., and Wagner, S., Encapsulating elastically stretchable neural interfaces: Yield, resolution, and recording/stimulation of neural activity. Advanced Functional Materials, 2012. **22**: p. 640-51.
16. Wagner, Size-dependent rupture strain of elastically stretchable metal conductors, Scripta Materialia 66 (2012) 919–922.
17. S. Wagner and S. Bauer, Materials for stretchable electronics, Lead article for the MRS Bulletin issue with the same title, vol. 37 (3), March 2012.

Manuscripts submitted or in preparation:

1. Choo, A.M., Miller, W.J., Chen, Y.C., Nibley, P., Goletiani, C., Morrison III, B., Kutzing, M.K., Firestein, B.L., Sul, J.Y., Haydon, P.G., and Meaney, D.F., Antagonism of astroglial purinergic signaling improves recovery from traumatic brain injury, submitted.
2. Wierzbicki, B., McManus, K., Choo, A.M., Mesfin, M., Kuo, E., Firestein, B.L. and Meaney, D.F. An accelerated Morris Water Maze test to assess dynamic state of hippocampal function. Submitted.
3. Ventre, S., Patel, T., Meaney, D.F., *In silico* and *in vitro* analysis of neural network activity patterns: Multiscale integration, Ann of Biomed Eng, in review.
4. O. Graudejus, Zheng Jia,Teng Li, and S. WaGoletiani, C., Firestein, B.L., Morrison III, B., Uric acid reduces cell death and preserved electrophysiological function after mechanical injury of organotypic brain slice cultures, in preparation.

7. Financial summary.

All funds have been expended with a grant balance of $0. Rutgers University Accounting Office will send the summary under separate mailing.

Subproject 1: Figures

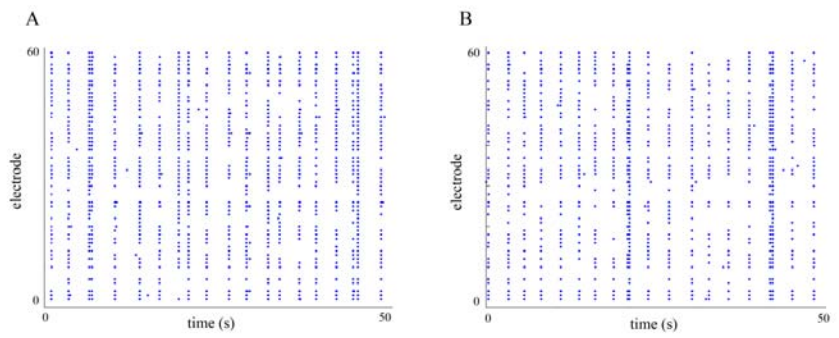

Figure 1: The ability of memantine to protect the synchronized firing between electrode pairs. A representative MEA for each condition is shown. SI=synchronization index. Column 1 shows the synchronization grids before drug treatment, column 2 shows the synchronization grids 24 hours after drug treatment, and column 3 shows the change in synchronization (CS) as a result of drug treatment. In the left and middle columns, a red color designates that the two electrodes have a high SI, indicating that both electrodes frequently record a spike within the same burst. A dark blue color designates little to no synchronization between the neurons whose action potentials are recorded on those electrodes. In the third column, a red or yellow color indicates an increase in the SI (positive CS), a pale green color represents no change in the SI, and a blue color represents a decrease in the SI (negative CS).

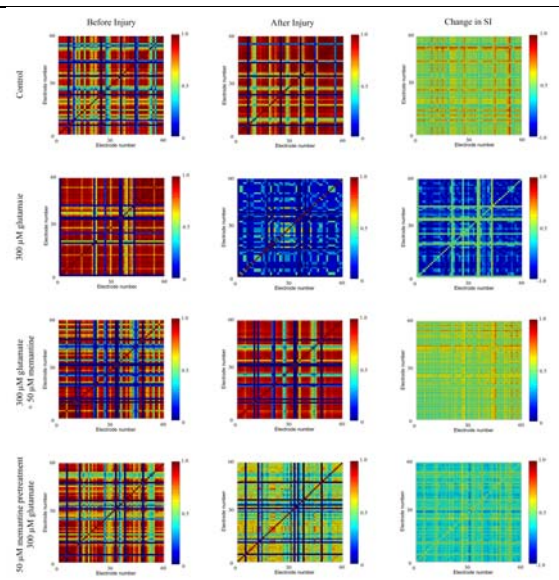

Figure 2: The effect of glutamate and memantine treatment on the average synchronization index value of electrodes. A representative MEA for each condition is shown. ASI = average synchronization index. The location of the ASI value for each electrode represents the actual physical location of the electrode on the MEA. Column 1 shows the ASI values prior to drug treatment, column 2 shows the ASI values 24 hours after drug treatment, and column 3 represents the change in the average synchronization of each electrode as a result of drug treatment. In the left and middle columns, a red color designates that that electrode has a high ASI, indicating that the neurons on that electrode fire in synchrony with neurons on other electrodes. A dark blue color designates that the neurons whose action potentials are recorded on that electrode do not fire with a high degree of synchrony with many neurons on other electrodes. In the third column, a yellow color indicates an increase in the ASI, a pale green color represents no change in the ASI, and a blue color represents a decrease in the ASI.

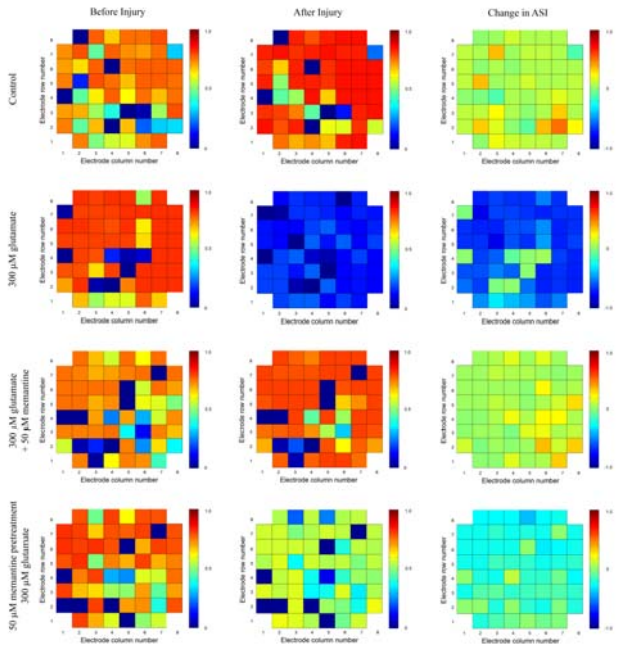

Figure 3: Memantine fully protects neurons from an overall loss in SI. Treatment with different memantine either during or prior to treatment with 300 µM glutamate results in complete protection from the overall loss of synchronization observed in cultures treated with glutamate alone. * = statistically different from control. ***p<0.001 determined by one-way ANOVA followed by Student-Newman-Keuls Multiple Comparison Test. Statistical analysis was performed on a per MEA basis (n=20 for control, n=21 for 300 µM glutamate, n=12 for concurrent 300 µM glutamate and 50 µM memantine treatment, n=12 for pretreatment with 50 µM memantine treatment followed by treatment with 300 µM glutamate).

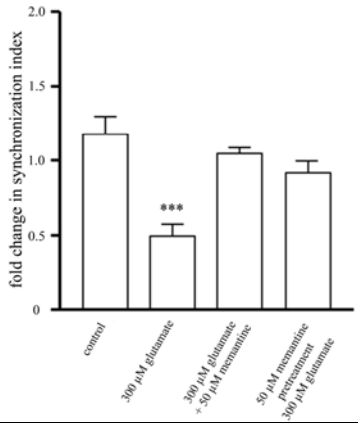

Figure 4: The initial synchronization between electrode pairs determines the ability of memantine to protect. Treatment with memantine at the same time as glutamate treatment is able to fully prevent against the loss of action potential synchrony observed in glutamate treated cultures. Treatment with memantine prior to glutamate treatment blocks the effects of glutamate treatment on the synchronization of electrode pairs that are initially weakly and moderately synchronized, but is unable to fully protect electrode pairs that are initially strongly synchronized. *= statistically different from control. # = statistically different from 300 µM glutamate. *** p<0.001, *p<0.05 determined by one-way ANOVA followed by Student-Newman-Keuls Multiple Comparison Test. Statistical analysis was performed on a per MEA basis (n=20 for control, n=21 for 300 µM glutamate, n=12 for concurrent 300 µM glutamate and 50 µM memantine treatment, n=12 for pretreatment with 50 µM memantine treatment followed by treatment with 300 µM glutamate).

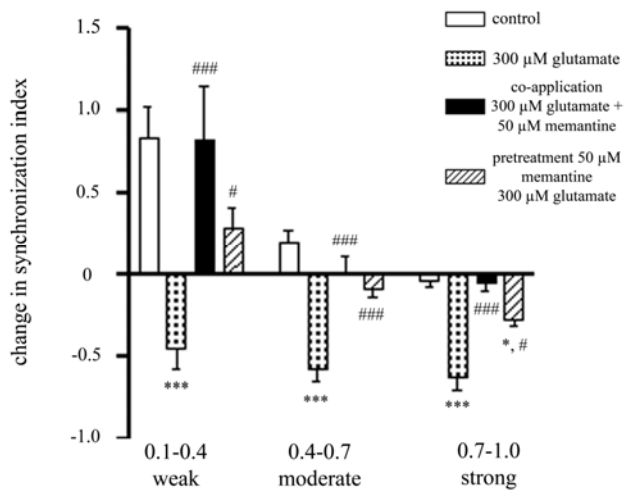

Figure 5: The change in burst duration after glutamate and memantine treatments. Cultures treated with 300 µM glutamate had a significant increase in average burst duration. Cultures treated with 50 µM memantine at the same time as 300 µM glutamate had no change in the average burst duration. Cultures pretreated with 50 µM memantine prior to glutamate treatment had a significant increase in burst duration. *= statistically different from control. # = statistically different from 300 µM glutamate. ***p<0.001, **p<0.01, *p<0.05 determined by one-way ANOVA followed by Student-Newman-Keuls Multiple Comparison Test. Statistical analysis was performed on a per MEA basis (n=20 for control, n=21 for 300 µM glutamate, n=12 for concurrent 300 µM glutamate and 50 µM memantine treatment, n=12 for pretreatment with 50 µM memantine treatment followed by treatment with 300 µM glutamate).

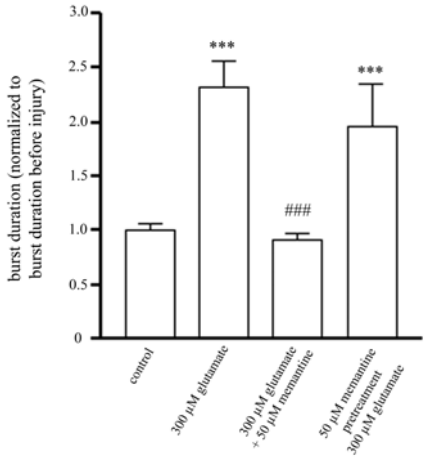

Figure 6: The effect of glutamate and memantine treatment on burst duration. Example SBEs before and after drug treatment for control cultures, cultures treated with 300 µM glutamate, cultures treated with 50 µM memantine at the same time as 300 µM glutamate, and cultures pretreated with 50 µM memantine followed by 300 µM memantine treatment. Each picture encompasses a single SBE. Each dot in the graphs represents a recorded spike.

Subproject 2: Figures

Columbia University:

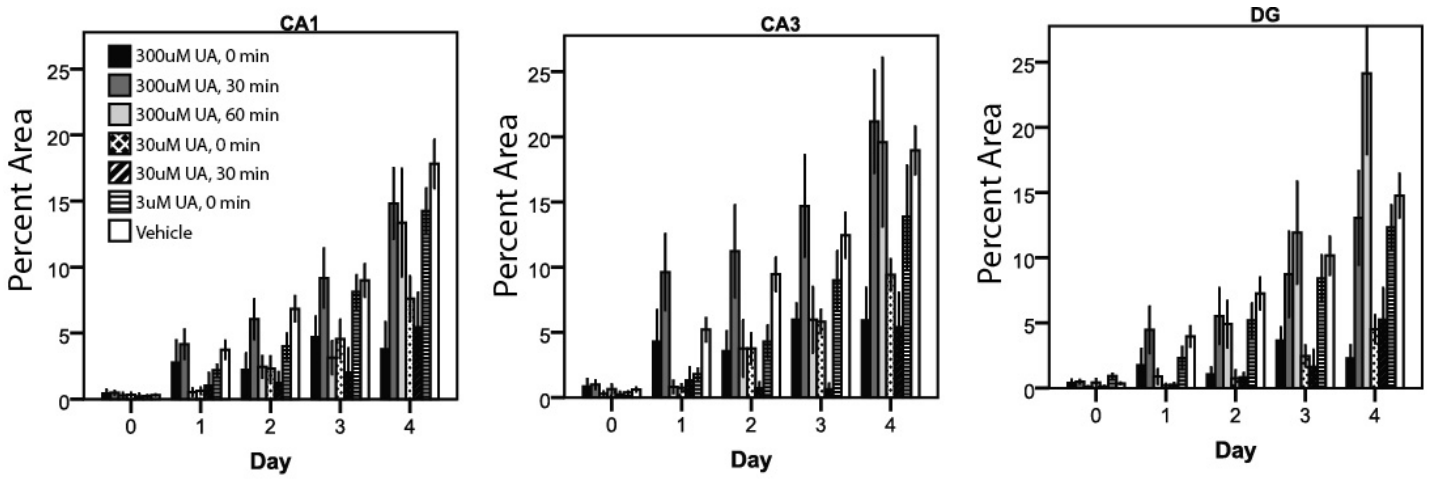

Figure 1 Uric acid significantly reduced cell death over time as measured by propidium iodide staining.

Table 1 Summary of statistical finding illustrated in Figure 1.

Region	Day of treatment	Vehicle vs UA 300 µM	Vehicle vs UA 300 µM 30 min delay	Vehicle vs UA 300 µM 60 min delay	Vehicle vs UA 30 µM	Vehicle vs UA 30 µM 30 min delay	Vehicle vs UA 3 µM
CA1	0						
	1						
	2					*↓	
	3					*↓	
	4	*↓			*↓	*↓	
CA3	0						
	1						
	2					*↓	
	3					*↓	
	4	*↓			*↓	*↓	
DG	0						*↓
	1						
	2				*↓	*↓	
	3				*↓	*↓	
	4	*↓			*↓	*↓	

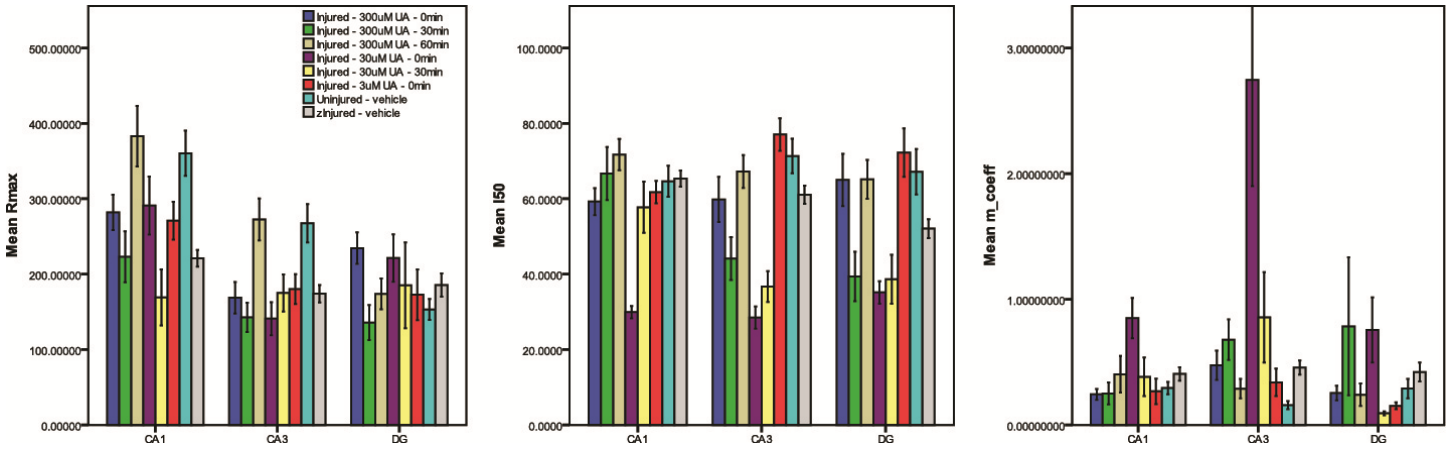

Figure 2 Uric acid treatment helped to preserve neuronal function as determined by evoked responses due to stimulation in the CA3 Shaffer collaterals and characterized by R_{max}, I_{50}, and m.

Table 2 Summary of statistical finding illustrated in Figure 2.

Rmax	Vehicle vs UA 300 µM	Vehicle vs UA 300 µM 30 min delay	Vehicle vs UA 300 µM 60 min delay	Vehicle vs UA 30 µM	Vehicle vs UA 30 µM 30 min delay	Vehicle vs UA 3 µM
CA1			*↑			
CA3			*↑			
DG						
I50						
CA1				*↓		
CA3				*↓	*↓	
DG						
m						
CA1				*↑		
CA3				*↑		
DG						

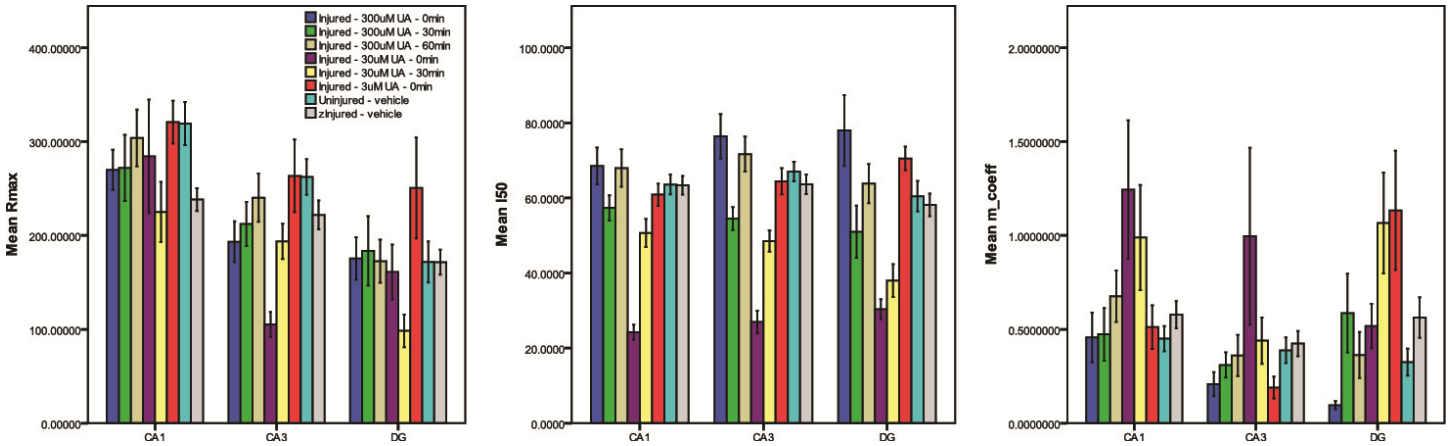

Figure 3 Uric acid treatment helped to preserve neuronal function as determined by evoked responses due to stimulation in the DG and characterized by R_{max}, I_{50}, and m.

Table 3 Summary of statistical finding illustrated in Figure 3.

Rmax	Vehicle vs UA 300 µM	Vehicle vs UA 300 µM 30 min delay	Vehicle vs UA 300 µM 60 min delay	Vehicle vs UA 30 µM	Vehicle vs UA 30 µM 30 min delay	Vehicle vs UA 3 µM
CA1						*↑
CA3						
DG						
I50						
CA1				*↓		
CA3				*↓		
DG	*↑			*↓		
m						
CA1				*↑		
CA3						
DG						*↑

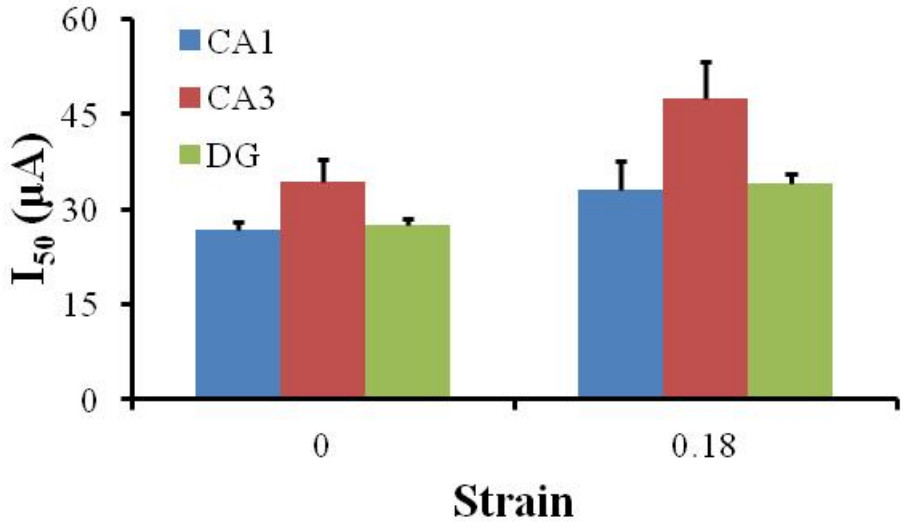

Figure 4 Quantification of I_{50} in CA1, CA3, and DG hippocampal regions after mechanical deformation. I_{50} increased in all regions after 18% strain stretch injury.

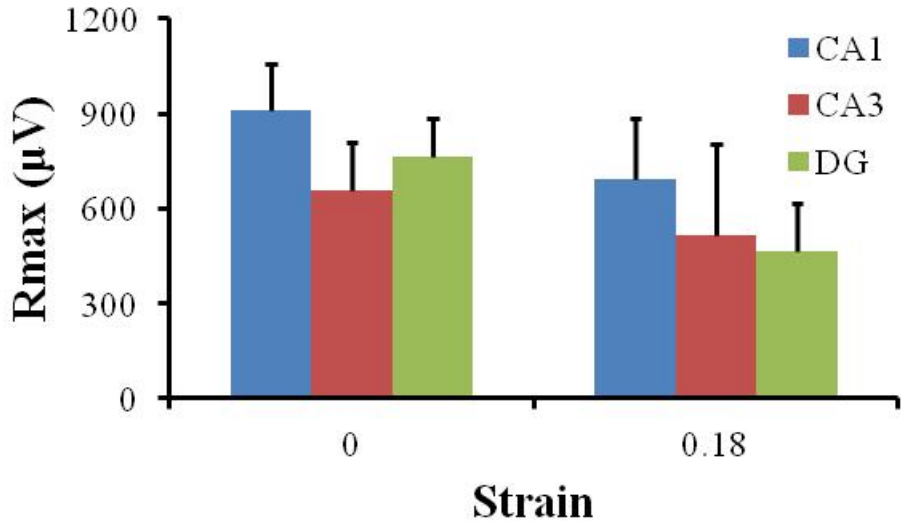

Figure 5 Quantification of R_{max} in CA1, CA3, and DG hippocampal regions after mechanical deformation. R_{max} decreased in all regions after 18% strain stretch injury.

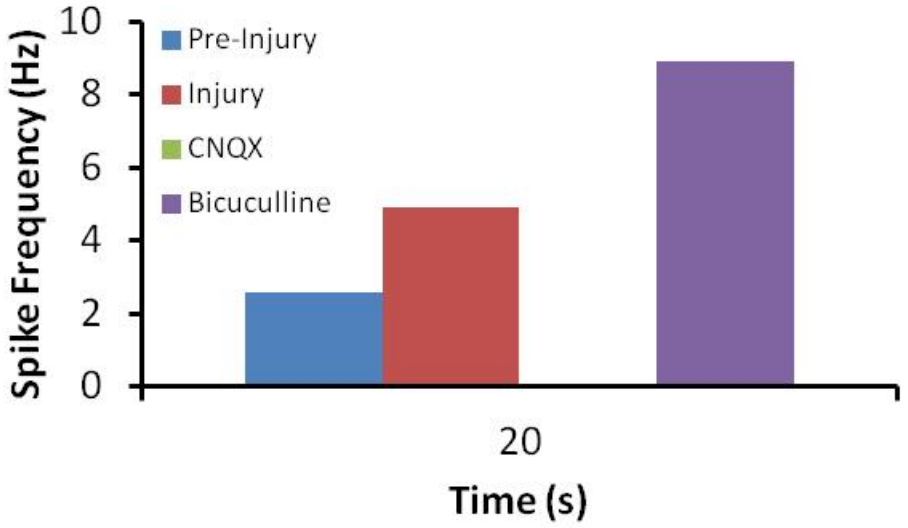

Figure 6 Quantification of population spike frequency after mechanical deformation and pharmacology. Spike frequency increased after 18% strain stretch injury compared to pre-injury, baseline levels. Within the same tissue slice, CNQX – an AMPA/kainate receptor antagonist – was then introduced, eliminating spike activity completely. After washout of CNQX, bicuculline – a $GABA_A$ receptor antagonist – was introduced, amplifying spike frequency.

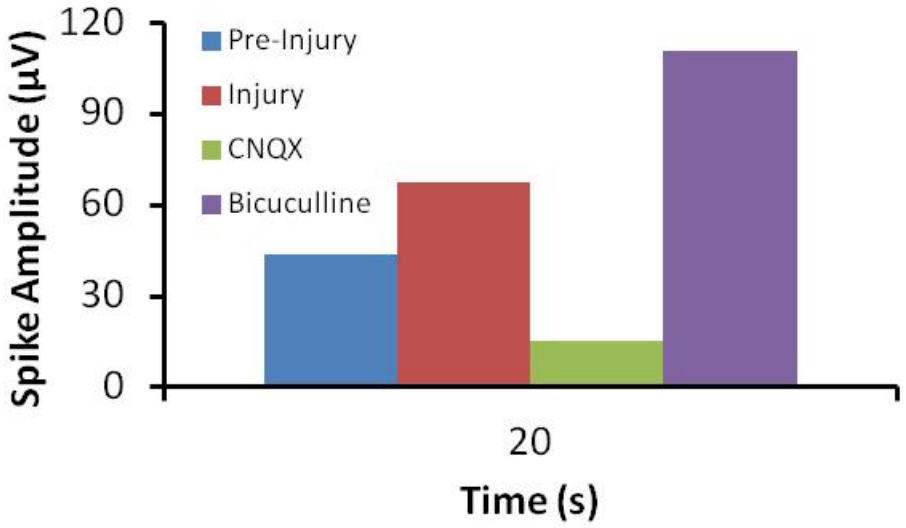

Figure 7 Quantification of population spike amplitude after mechanical deformation and pharmacology. Spike amplitude increased after 18% strain stretch injury compared to pre-injury, baseline levels. Within the same tissue slice, CNQX – an AMPA/kainate receptor antagonist – was then introduced, nearly abolishing spike activity. After washout of CNQX, bicuculline – a $GABA_A$ receptor antagonist – was introduced, amplifying spike frequency.

Princeton University:

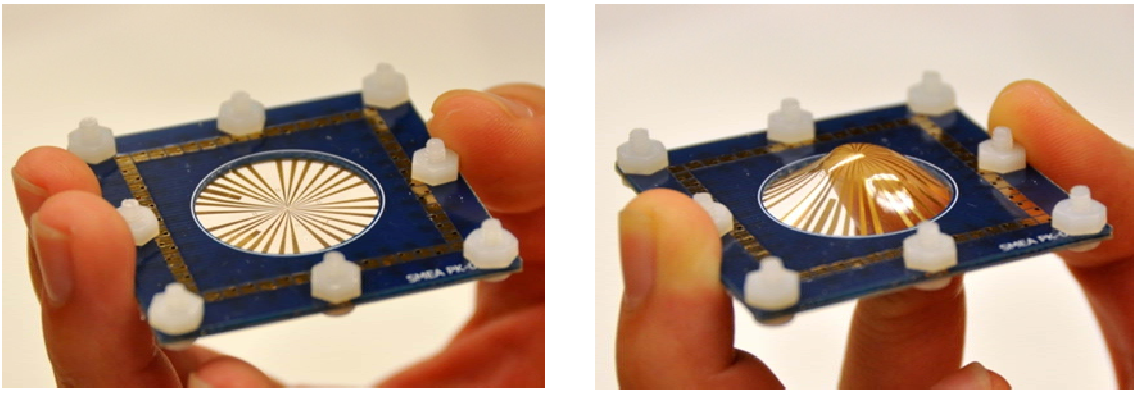

Figure 1. Stretchable microelectrode array in (left) its relaxed state (left) and (right) while stretched. The core of the array is a clear silicon membrane with rubber-like properties, that has stretchable electric conductors patterned on it. The central part of the array is visible in the circular opening made in the two printed wiring boards between which the membrane is clamped. The two wiring boards are held together by eight plastic screws and nuts. The electrical conductors continue between the two wiring boards and reach the contacts that are arrayed in a square along the perimeter of the top printed wiring board. Electronic equipment makes contact to the contact pads that form the square.

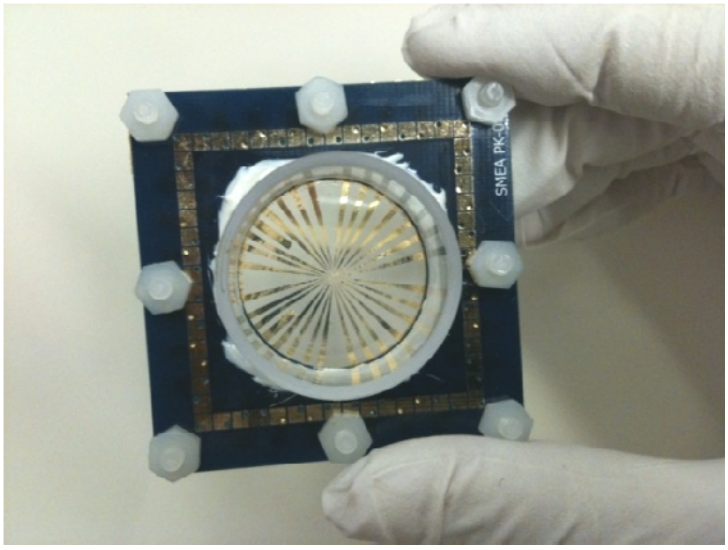

Figure 2. Top view of a stretchable microelectrode array with a nalgene cylinder, attached to the array such as to form a growth well.

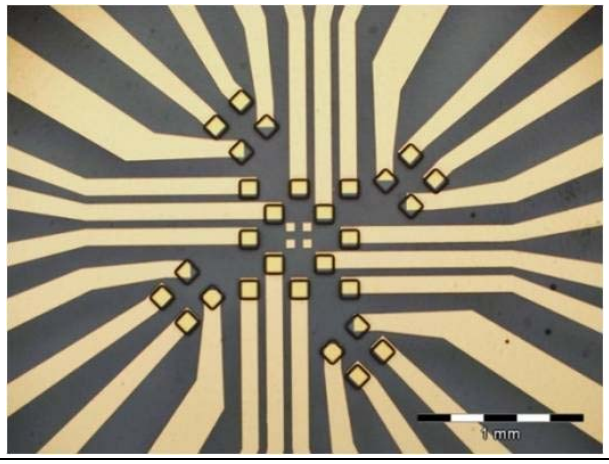

Figure 3. Optical micrograph of the central portion of a microelectrode array. The squares at the tips of each conductor are the active electrodes; there the conductors are not coated with the transparent electrical insulator. The full length of the scale bar at the lower right is 1 mm.

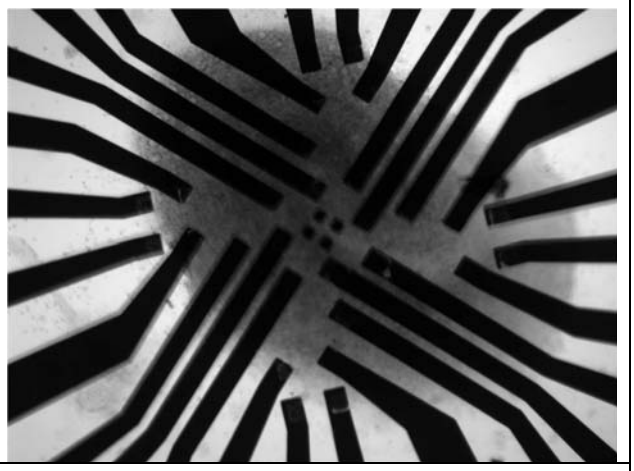

Figure 4. Optical micrograph of a hippocampal tissue culture on a stretchable microelectrode array.

Subproject 3: Figures

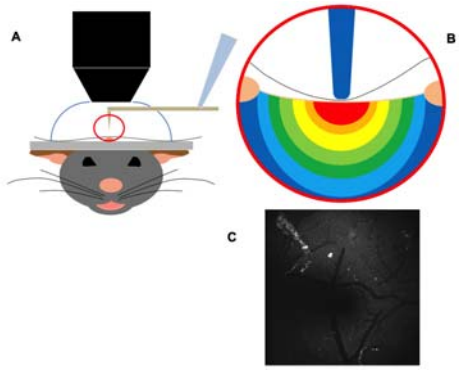

Figure 1 – The microcortical impact technique (a) is a technique to study the response of astrocytes within the cortex to a localized impact that mimics traumatic brain injury. The stress patterns in the cortex (colorized in B) are maximal at the tip of the small (200 um) impactor tip. The tip is adjusted to be in the center of the image plane (light microscopy image shown in C), and the viewing field for the time lapse multiphoton imaging appears 200 um below the cortical surface.

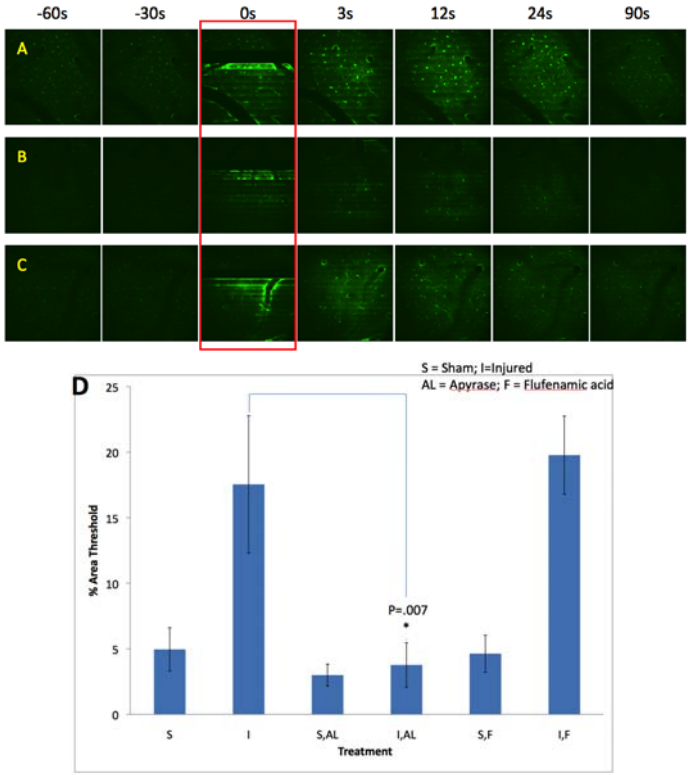

Figure 2 – The response of astrocytes within the cortex to mechanical trauma is dependent upon purinergic receptors. Fluo-4, a calcium sensitive fluorescent indicator dye, was loaded into astrocytes prior to impact. A. At the time of impact (0 s), there is an immediate response followed by a rapidly expanding area of astrocytes showing a significant increase in Fluo-4 fluorescence, indicating a specific increase in cytosolic calcium within the astrocyte population. B. Treating the cortex with apyrase to enhance the enzymatic degradation of ATP leads to a significant reduction in the number of astrocytes activated following impact. C. Alternatively, inhibiting gap junctions with flufenamic acid did not change the area of activated astrocytes. D. Measuring the extent of the increase in astrocyte intracellular calcium shows a significant reduction only for apyrase treatment, showing that immediate intercellular communication in astrocytes following traumatic injury to the cortex is mediated by purinergic receptors.

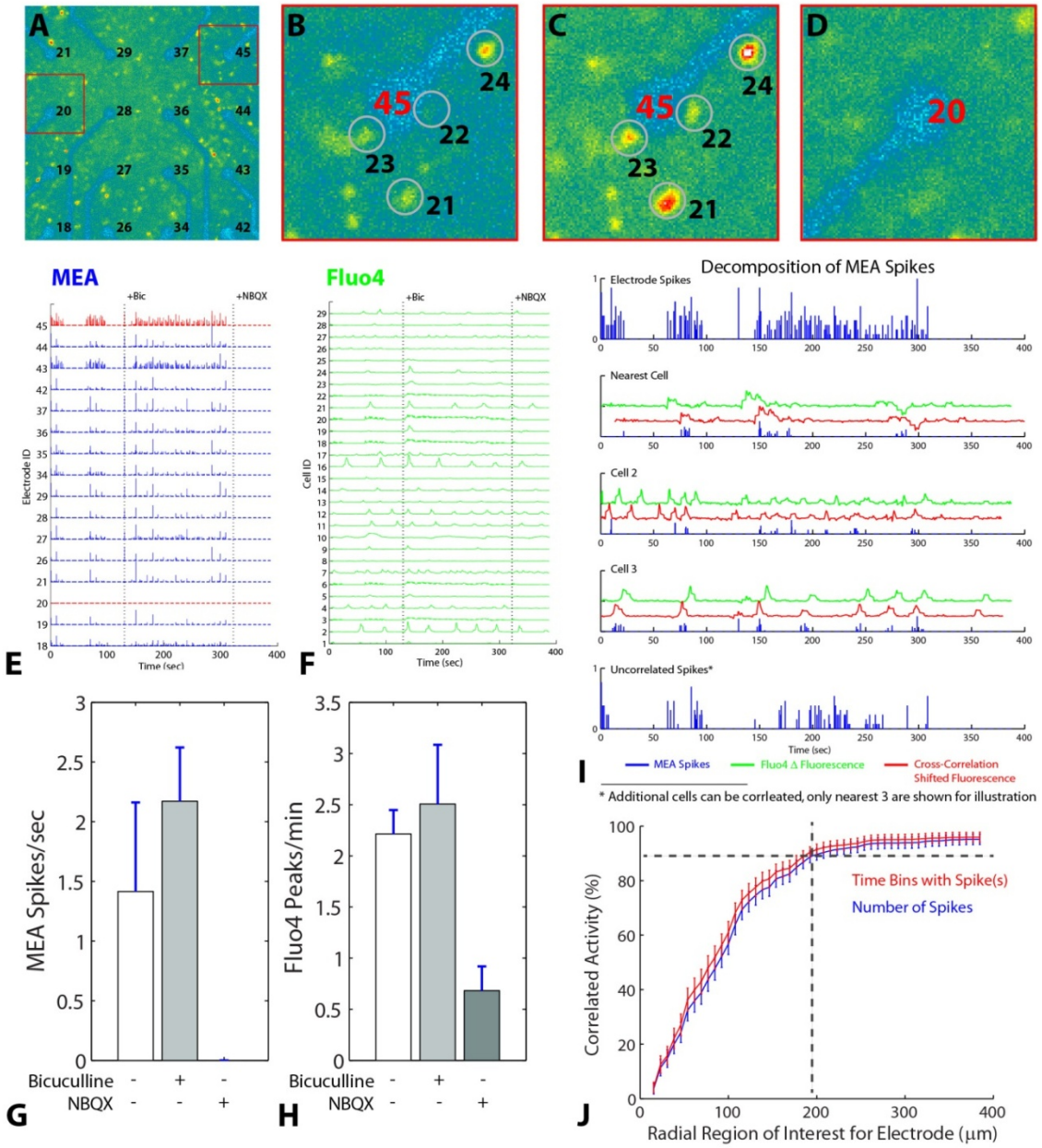
A
B
C
D
MEA
Fluo4
+Bic
+NBQX
Electrode ID
Cell ID
Time (sec)
E
F
Decomposition of MEA Spikes
Electrode Spikes
Nearest Cell
Cell 2
Cell 3
Uncorrelated Spikes*
MEA Spikes
Fluo4 Δ Fluorescence
Cross-Correlation Shifted Fluorescence
I
* Additional cells can be correlated, only nearest 3 are shown for illustration
MEA Spikes/sec
Fluo4 Peaks/min
Bicuculline
NBQX
G
H
Correlated Activity (%)
Time Bins with Spike(s)
Number of Spikes
Radial Region of Interest for Electrode (μm)
J

FIGURE 4

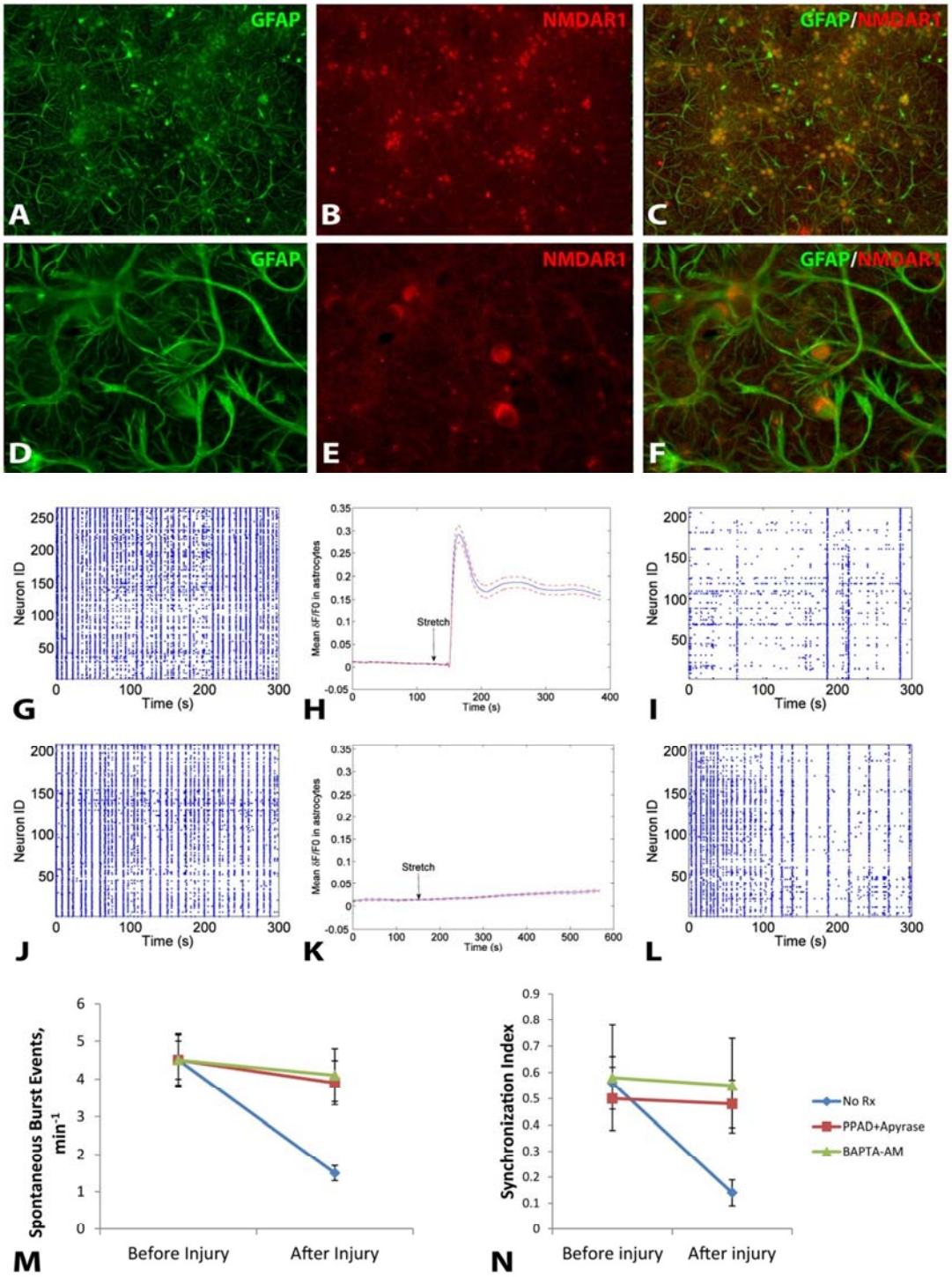
GFAP
NMDAR1
GFAP/NMDAR1
A
B
C
D
E
F
Neuron ID
Time (s)
Mean ΔF/F0 in astrocytes
Stretch
G
H
I
J
K
L
Spontaneous Burst Events, min-1
Before Injury
After Injury
M
Synchronization Index
Before injury
After injury
N
No Rx
PPAD+Apyrase
BAPTA-AM

FIGURE 5

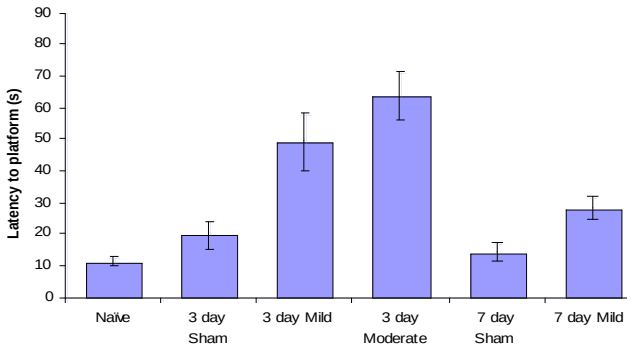

Figure 6 – Accelerated Morris Water Maze (MWM) testing reveals significant deficits in animals receiving a mild and moderate cortical impact injury 3d and 7d after injury.

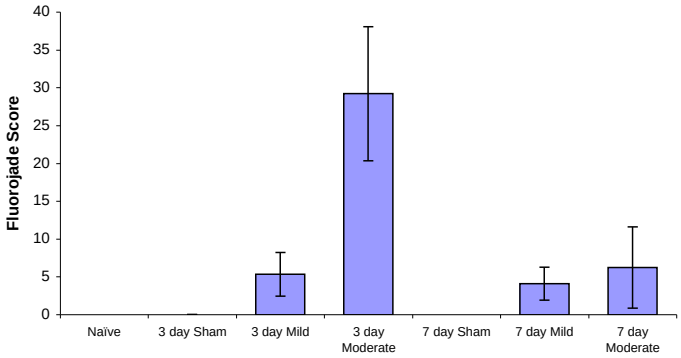

Figure 7 – Flourojade labeling is a method to detect degenerating neurons in the brain after cortical impact injury. Although a substantial amount of degenerating neurons are apparent 3d after injury, this degeneration is significantly less in the moderate injury level at 7d postinjury.

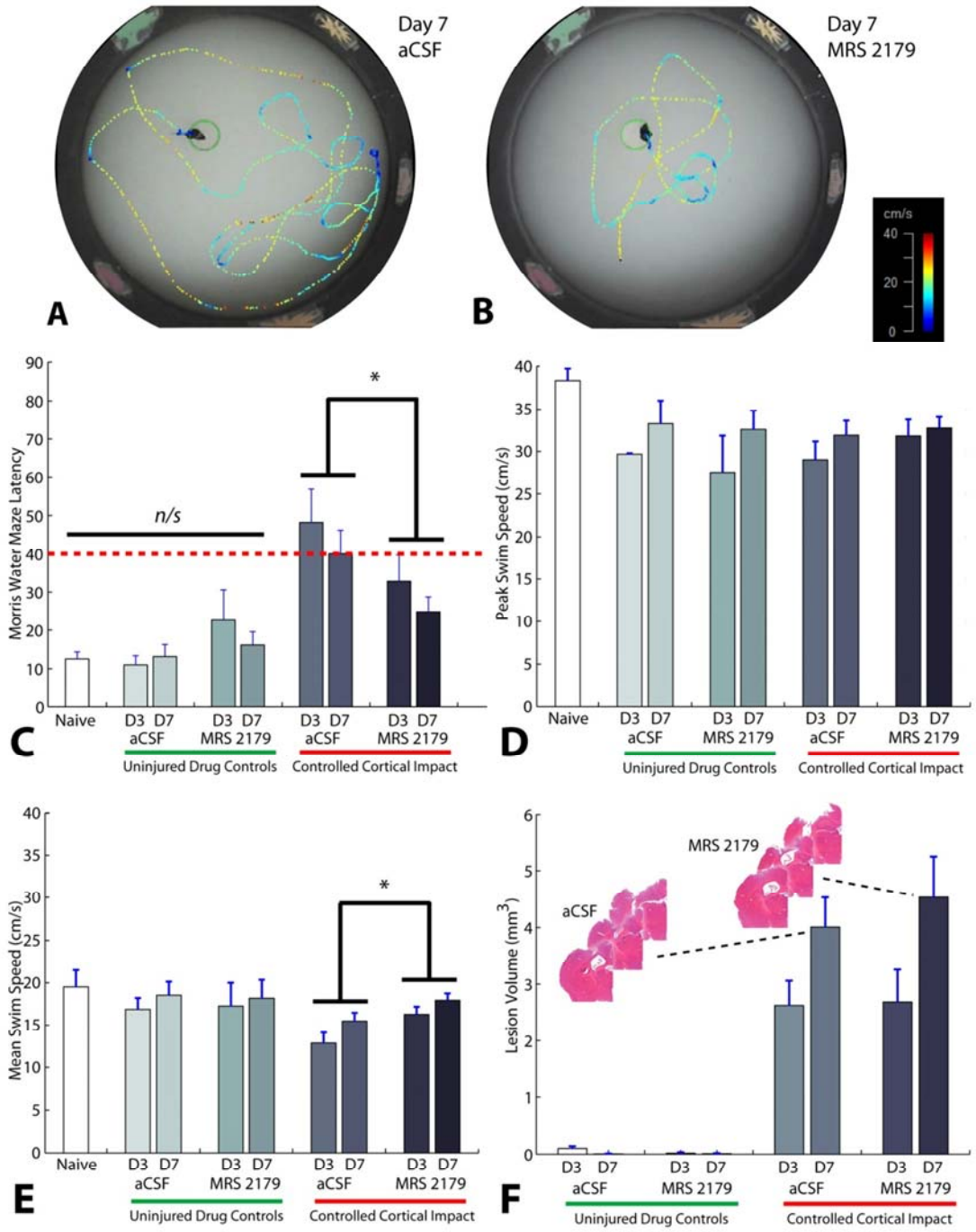
Day 7
aCSF
Day 7
MRS 2179
cm/s
40
20
0
A
B
Morris Water Maze Latency
n/s
*
Naive
D3 D7
aCSF
D3 D7
MRS 2179
D3 D7
aCSF
D3 D7
MRS 2179
Uninjured Drug Controls
Controlled Cortical Impact
C
Peak Swim Speed (cm/s)
D
Mean Swim Speed (cm/s)
E
Lesion Volume (mm3)
MRS 2179
aCSF
F

FIGURE 8

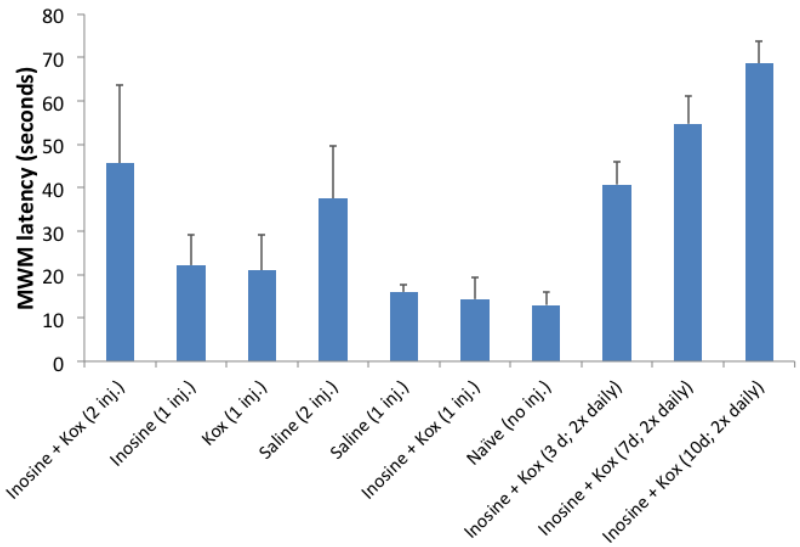

FIGURE 9

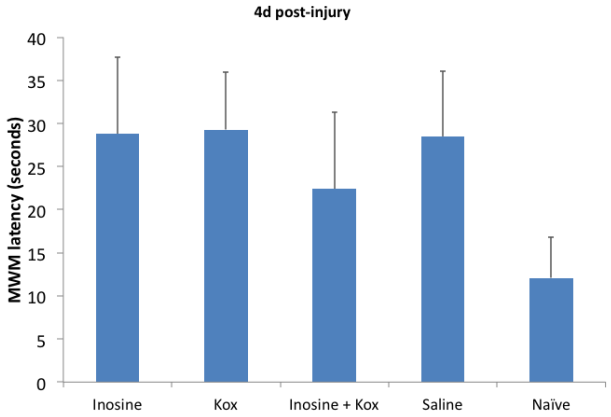

FIGURE 10

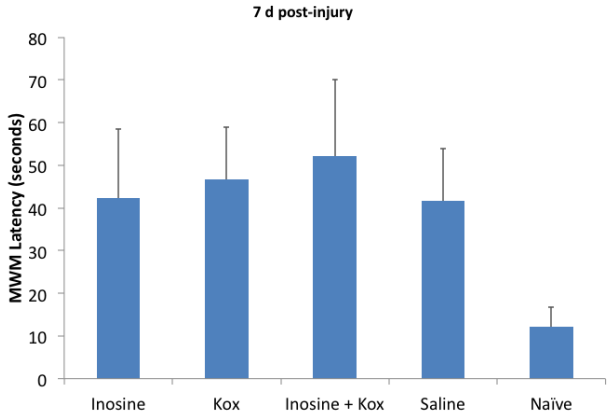

Figure 11